https://doi.org/10.5194/egusphere-2026-67
Preprint. Discussion started: 23 February 2026

An antiplane strain model for evaluating shear-margin stability (Ortholine v1.0)

Jenny Suckale[1,2] and Cooper W. Elsworth[1]

[1]Department of Geophysics, Stanford University, 397 Panama Mall, Stanford CA 94305, USA.
[2]Institute for Computational and Mathematical Engineering, Stanford University, 397 Panama Mall, Stanford CA 94305, USA.

Correspondence: Jenny Suckale (jsuckale@stanford.edu)

Abstract. Shear margins—the lateral boundaries of ice streams and glaciers—play a key role in the mass balance of our ice sheets. In glaciers, shear margins are often controlled by topography, whereas in ice streams they are inherently dynamic and can migrate. Margin migration alters the width of fast-moving ice and thus the force balance that controls ice speed and mass loss. Quantifying whether a shear margin is stable or prone to migration is hence important for estimating the future mass balance, but requires understanding the processes governing its current position. Numerous englacial and subglacial processes may contribute, including shear heating, fabric development, basal topography, lithology, and hydrology. Although the potential importance of these processes has been established, we currently lack models aimed at evaluating their relative importance at a specific field site and we aim to fill this gap. Here, we introduce "Ortholine", an antiplane-strain free-boundary model developed to evaluate the relative importance of different englacial and subglacial processes in controlling a specific shear-margin location. By focusing on the cross-sectional force balance of ice streams, Ortholine complements commonly used flow-line models. After deriving and verifying Ortholine, we outline the four key steps for applying it to a field site, using Institute Ice Stream in the Weddel Sea Sector, Antarctica, as a proof-of-concept. We have selected Institute Ice Stream as an example, because of its intermediate complexity and the sufficient availability of field data to guide the model setup.

1 Introduction

Ice streams and glaciers together account for the majority of mass loss from the Antarctic continent (Bamber et al., 2000). Their mass loss depends not only on the speed of the ice, but also on the width of the fast-flowing zone (Raymond, 1996). Observations show that shear margins can move, either gradually (Harrison et al., 1998; Bindschadler and Vornberger, 1998; Echelmeyer and Harrison, 1999; Clarke et al., 2000) or abruptly (Catania et al., 2006). It is less clear how commonly shear margins move, partly because shear margins are difficult to pinpoint on satellite data due to heavy crevassing, and partly because migration rates on the order of meters per year are challenging to resolve. If shear margins were to move, the consequences for sea-level rise projections could be significant because the outward motion of a shear margin not only increases the width, but also the speed of fast moving ice (Raymond, 1996).

The puzzling variability of observed shear-margin behavior raises the question of what physical processes control shear-margin mobility and how these processes might be affected by evolving climatic conditions. Previous models have improved

https://doi.org/10.5194/egusphere-2026-67
Preprint. Discussion started: 23 February 2026

our understanding of how thermal (Schoof, 2004, 2012; Suckale et al., 2014; Perol et al., 2015; Haseloff et al., 2015), and hydrological (Perol and Rice, 2015; Platt et al., 2016; Elsworth and Suckale, 2016) processes at the base of the ice contribute to the stability of shear margins. However, most of these models consider only a single shear margin assuming symmetric and idealized ice streams sliding over a homogeneous bed, inspired by the Siple Coast Ice Streams that are characterized by low topography, complex subglacial hydrology and widespread sediment deposits (e.g., Perol et al., 2015; Suckale et al., 2014; Elsworth and Suckale, 2016).

Figure 1 highlights the location of the Siple Coast Ice Streams superimposed on the shear-strain rate field of the Antarctic Ice Sheet as estimated from Landsat 8 satellite data by Alley et al. (2018). It also shows several other locations where shear-margin properties are likely controlled by other physical processes than in the Siple Coast, ranging from topography at Lambert Glacier (Sanderson et al., 2023), to spatial variations in subglacial conditions at Institute Ice Stream (Siegert et al., 2016), and possibly a combination of all of these at Thwaites Glacier. Thwaites Glacier is particularly relevant, because it is a case where one shear margin might be more prone to migration than the other (MacGregor et al., 2013) and because of its prominent contribution to current sea-level rise (e.g., Holland et al., 2023).

The goal of this study is to advance our ability to evaluate the relative importance of different englacial and subglacial processes in controlling a specific shear-margin location by developing an easily portable model, “Ortholine”. Methodologically, Ortholine attempts to strike a balance between the appealing simplicity of idealized shear-margin models that have contributed to our theoretical understanding (e.g., Jacobson and Raymond, 1998; Schoof, 2004; Suckale et al., 2014; Haseloff et al., 2015; Perol and Rice, 2015; Elsworth and Suckale, 2016; Haseloff et al., 2019) and the inevitable complexity of the field sites for which we aim to assess shear-margin stability. We build on the cross-sectional, free-boundary formulation of Schoof (2006b, a), which allows us to determine the slipping regions at the ice-bed interface self-consistently from an integrated force balance.

Our model design is inspired by the scientific successes of simple flow-line models pioneered by Nye (1957) and widely adopted by the scientific community in the 1980s (e.g., Hooke et al., 1979; Morland and Johnson, 1980; Reeh and Paterson, 1988). Flow-line models neglect shear margins and thereby reduce a three-dimensional problem to plane strain along the main flow direction. A complementary point of view that allows for an explicit focus on shear margins is to assume antiplane strain and instead neglect longitudinal stresses (e.g., Jacobson and Raymond, 1998). The name of our model, “Ortholine”, is motivated partly by the orthogonal orientation of our model domain to the main flow line and partly by its conceptual orthogonality to flow-line models. Ortholine allows researchers to focus on an aspect of ice dynamics, the shear margin, that is neglected in flow-line models, justifying its conceptual orthogonality to flow-line models.

Previous antiplane strain models of shear margins simplify the domain as symmetric and assume a flat basal topography (Jacobson and Raymond, 1998; Schoof, 2004; Suckale et al., 2014; Perol and Rice, 2015; Haseloff et al., 2015; Elsworth and Suckale, 2016). Instead, we implement a body-fitted mesh using the GMESH package (Geuzaine and Remacle, 2009) that can capture variable subglacial topography in the model domain. We also allow for heterogeneous and basal conditions representative of perfectly plastic sediment behavior (Tulaczyk et al., 2000b; Kamb, 2001), velocity-strengthening hard rock sliding laws (Weertman, 1957), and regularized Coulomb sliding over hard rock (Schoof, 2005) while maximizing computational ef-

https://doi.org/10.5194/egusphere-2026-67
Preprint. Discussion started: 23 February 2026

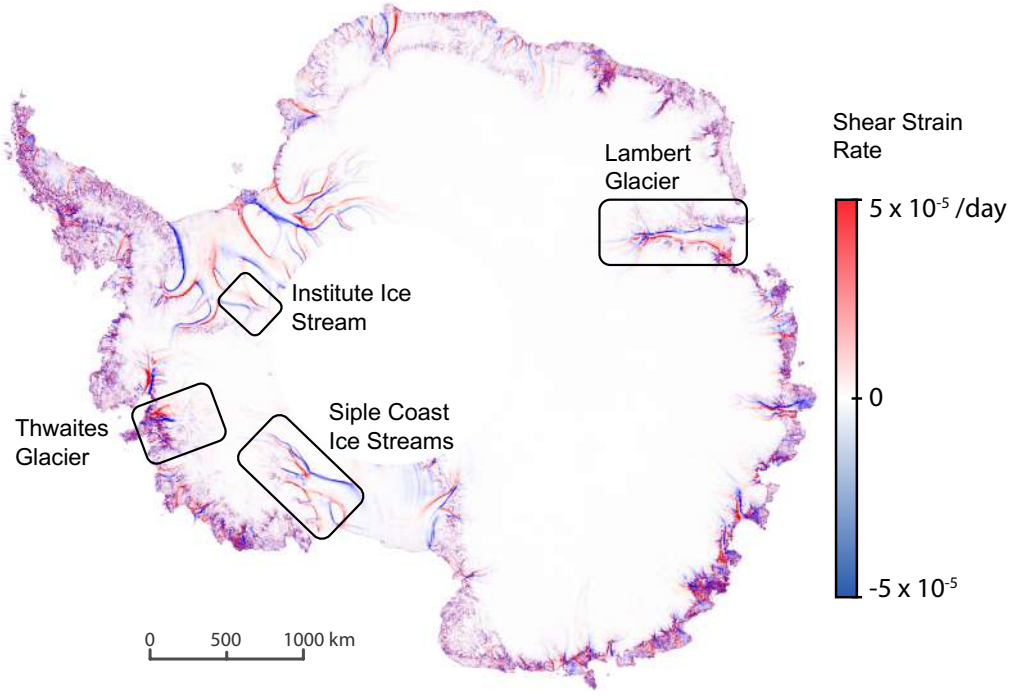

Figure 1. Map of the shear strain rate estimated from the satellite-derived velocity field of the Antarctic ice sheet based on Landsat 8 satellite data by Alley et al. (2018). Superimposed are the locations where shear margins might be controlled by different physical processes. Figure created by Cooper W. Elsworth.

ficiency. Including these heterogeneities implies that the plane of antiplane stress might not be identical to the cross-section of the ice stream. We have developed an accompanying algorithm to compute the appropriate model plane from surface velocities.

Although Ortholine is intended as a general framework that can be easily adapted to any given field site, we detail the steps to apply it for the case of Institute Ice Stream in the Weddel Sea Sector, Antarctica (see Fig. 1). Institute Ice Stream represents a field setting of moderate complexity that shares similarities with the Siple Coast, such as low overall driving stresses and a widespread unconsolidated sediment layer (Bingham and Siegert, 2007). Radioecho sounding surveys map out a mildly varying topography and suggest the existence of a distinct transition between hardrock and saturated sediments beneath the ice stream (Siegert et al., 2016). From a dynamic point of view, Institute Ice Stream has attracted attention because it is located on a reverse-sloping bed with few pinning points (Bingham and Siegert, 2007; Ross et al., 2012), making it prone to the marine ice-sheet instability (Weertman, 1974; Thomas, 1979; Schoof, 2007; Jamieson et al., 2012).

2 Methods

We develop a thermomechanical model of an ice stream cross section oriented orthogonal to the flow line. Instead of preimposing the margin positions, we solve a free-boundary problem to slipping portion of the bed based on an integrated force

https://doi.org/10.5194/egusphere-2026-67
Preprint. Discussion started: 23 February 2026

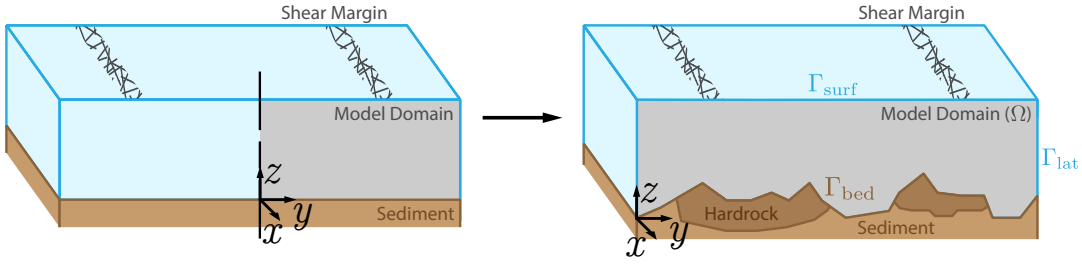

Figure 2. Model domain of previous models as compared to Ortholine. Both model approaches neglect variability in along-flow direction, x. Advancing on previous idealized models (left), Ortholine captures the entire width of the zone of fast-moving ice including both shear margins and allows for spatially varying lithology, subglacial hydrology and basal topography (right). Figure created by Cooper W. Elsworth.

balance across the domain based on the derivation by Schoof (2006b). We formulate the governing equations of ice flow for three different subglacial boundary conditions representative of failing sediments, locked sediments, and hard-bed sliding. We then convert the free-boundary problem to a convex optimization problem and solve it through the Disciplined Convex Programming framework (Grant and Boyd, 2014).

2.1 Governing Equations

Our free-boundary model extends the mechanical model by Schoof (2006b) to include thermo-mechanical effects. To reduce the complexity of the 3-D geometry, we neglect variability in the downstream direction ($d/dx \approx 0$), with the ice moving in the positive x direction, shown in Figure 2b. Neglecting downstream variability reduces the momentum balance to

$$-\nabla \cdot \left(\eta(T)|\nabla u|^{1/n-1}\nabla u\right) = \rho g \sin\alpha \qquad \text{on} \qquad \Omega, \tag{1}$$

with anti-plane speed, u, temperature-dependent ice viscosity, $\eta(T)$, power-law exponent, n, ice density, ρ, gravitational acceleration, g, and surface slope, α. A typical non-Newtonian Glen's rheology would entail $n = 3$ (Glen, 1955).

We assume that the ice thickness is constant with a stress-free surface,

$$-\eta(T)|\nabla u|^{1/n-1}u_n = 0 \qquad \text{on} \qquad \Gamma_{\text{surf}}, \tag{2}$$

where $u_n = \frac{\partial u}{\partial n}$ where n is the unit normal to the interface. Additionally, the domain has stress-free lateral bounds,

$$-\eta(T)|\nabla u|^{1/n-1}u_n = 0 \qquad \text{on} \qquad \Gamma_{\text{lat}}. \tag{3}$$

The basal traction at the bed,

$$-\eta(T)|\nabla u|^{1/n-1}u_n = \tau_b(x, y, u) \qquad \text{on} \qquad \Gamma_{\text{bed}}, \tag{4}$$

https://doi.org/10.5194/egusphere-2026-67
Preprint. Discussion started: 23 February 2026

captures regions of water-saturated sediments that abide by Coulomb Plasticity as observed experimentally (Tulaczyk et al., 2000a) with,

$$\tau_b = fN + c \qquad u > 0 \quad \text{(failing)} \tag{5}$$

$$\tau_b \leq fN + c \qquad u = 0 \quad \text{(locked)} \tag{6}$$

dependent on effective pressure, $N = \sigma_n - p$, where σ_n is the overburden, p the pore pressure, f the friction factor and c the cohesion of the sediment.

For the portion of the subglacial bed that consists of hardrock, we assume that the basal traction follows a sliding law,

$$\tau_b = \beta^2 |u|^m \tag{7}$$

dependent on the downstream ice speed, u, to the power m. This sliding law can represent three different regimes: velocity-strengthening behavior, $m > 0$, as might arise when sliding over bumps without cavitation (e.g., Weertman, 1957); velocity-weakening behavior, $m < 0$, potentially indicative of bed bumps with cavitation (e.g., Lliboutry, 1968); and regularized Coulomb sliding over hard rock, $m = 0$ (e.g., Schoof, 2005). Of these three possibilities, velocity-weakening behavior (Lliboutry, 1968; Zoet and Iverson, 2016) with $m < 0$, is unstable when applied to the entire or most of the hard rock bed. We therefore do not consider this limit in our simulations.

We assume that the temperature distribution in the ice column is driven by diffusion of shear heating,

$$-\nabla \cdot (k \nabla T) = 2\tau_E(u)\dot{\epsilon}_E(u), \quad T < T_{\text{melt}}, \tag{8}$$

with thermal conductivity, k, effective stress, $\tau_E(u)$, effective strain rate, $\dot{\epsilon}_E(u)$, and pressure melting point, T_{melt}. The boundary conditions are a fixed surface temperature, T_s,

$$T = T_s \qquad \text{on} \qquad \Gamma_{\text{surf}}, \tag{9}$$

no flux lateral bounds,

$$-k\nabla T = 0 \qquad \text{on} \qquad \Gamma_{\text{lat}}, \tag{10}$$

and constant geothermal heat flux, G_{geo}, at the bed,

$$-k\nabla T = G_{\text{geo}} \qquad \text{on} \qquad \Gamma_{\text{bed}}. \tag{11}$$

The primary difficulty in solving these governing equations arises from the unknown location and extent of the slip zone. When sliding occurs over perfectly plastic sediment, the slip zone ends at the point where the sediments transition from failing to locking, but the location of these transition points depends on the integrated force-balance of the ice stream. Without the location of the known transition points *a priori*, the solution of the governing equations includes both the depth-dependent ice speed and the location of the boundary conditions. Similarly, for the thermal model shear heating occurs until the melting point

https://doi.org/10.5194/egusphere-2026-67
Preprint. Discussion started: 23 February 2026

is reached, without regions of temperate ice known *a priori*. These types of free-boundary, partial differential equations can be solved as a variational inequality (Schoof, 2006b; Friedman, 2010).

The variational form of the mechanical free-boundary problem is derived in Schoof (2006b). In the variational formulation, solving the anti-plane momentum balance, Eq. 1, becomes equivalent minimizing the energy functional, $J(u)$, subject to the constraint that flow occurs only in the downstream direction:

$$\text{minimize} \qquad J(u) = \frac{1}{p}\int_{\Omega} \eta(T)|\nabla u|^p + \int_{\Gamma_{\text{bed}}} \tau_b|u| - \int_{\Omega} \rho g \sin\alpha u \tag{12}$$

$$\text{subject to} \qquad v \geq 0. \tag{13}$$

To simplify the notation, we set $p = 1 + 1/n$. The energy functional, $J(u)$, has been proven to be convex in $v \geq 0$, and unique when a solution exists (Schoof, 2006b).

We use the same method to develop a variational inequality for englacial temperature in the domain. We define the thermal energy functional, $L(T)$, which we minimize subject to the constraint that the temperature can not exceed the pressure melting point:

$$\text{minimize} \qquad L(T) = \frac{1}{2}\int_{\Omega} k|\nabla T|^2 - \int_{\Gamma_{\text{bed}}} G_{\text{geo}} T - \int_{\Omega} 2\tau_E(u)\dot{\epsilon}_E(u)T \tag{14}$$

$$\text{subject to} \qquad T \leq T_{\text{melt}}. \tag{15}$$

Our model extends the approach of Meyer and Minchew (2018), a one-dimensional free-boundary analytical solution for the temperature field in an ice column, to two dimensions.

2.2 Numerical Method

As described above, we reformulate the initial governing equations as a set of constrained minimizations problems that are convex in the anti-plane speed, u, and temperature, T. For a given domain, we solve these optimization problems by discretizing the domain and solving the convex minimization numerically. We begin by discretizing the mechanical-energy functional, described by Eq. 12 on a domain, Ω, with an arbitrary triangulation consisting of elements, τ, and boundary edges, γ,

$$J(u) = \frac{1}{p}\sum_{\tau}\int_{\tau} \eta(T)|\nabla u|^p + \sum_{\gamma}\int_{\gamma} \tau_b|u| - \sum_{\tau}\int_{\tau} \rho g \sin\alpha u. \tag{16}$$

Choosing a piecewise-linear basis, ϕ_i, on each element with nodal weight function, v_i, the semi-discretized energy functional becomes

$$J(u_i) = \frac{1}{p}\sum_{\tau}\eta(T)\int_{\tau}\left|\sum_{i=1}^{3} u_i \nabla\phi_i\right|^p + \sum_{\gamma}\sum_{i=1}^{2} u_i \int_{\gamma} \tau_b\phi_i - \rho g\sin\alpha \sum_{\tau}\sum_{i=1}^{3} u_i \int_{\tau}\phi_i. \tag{17}$$

The next step is to fully discretize each term of the energy functional, while ensuring that each term follows the convex composition rules of Disciplined Convex Programming described in Grant et al. (2006). Disciplined Convex Programming is

https://doi.org/10.5194/egusphere-2026-67
Preprint. Discussion started: 23 February 2026

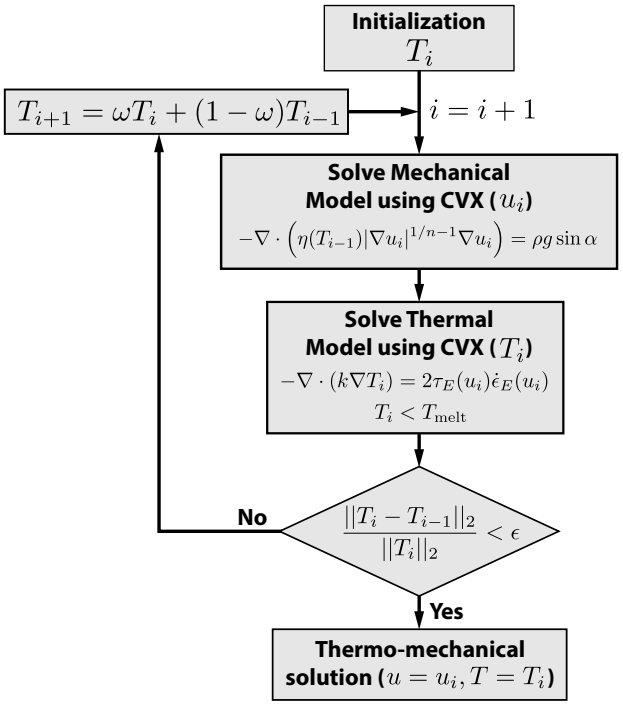

Figure 3. Flowchart of our thermo-mechanical coupling scheme. We first solve the mechanical and thermal free-boundary problems separately using CVX (Grant and Boyd, 2014). We couple the two solutions with under-relaxation of the temperature field in a Newton-Raphson iteration of the mechanical model. We iterate until the residual falls below a prescribed value, ϵ. Figure created by Cooper W. Elsworth.

a framework for specifying convex minimization problems algorithmically, which can then be solved by generalized, efficient numerical methods (Grant and Boyd, 2014).

To demonstrate how the minimization problem in Eq. 17 can be reformulated to be amenable to the CVX algorithm, where CVX is short for 'convex' (Grant and Boyd, 2014), each of the terms in the energy functional must be decomposed into the composition of convex operators. We define each term in the energy functional described by Eq. 17 as,

$$J(v_i) = J_A(v_i) + J_B(v_i) + J_C(v_i). \tag{18}$$

For example, the $J_A(v_i)$ on a single element, τ, becomes,

$$J_A(v_i) = \frac{1}{p}\eta \int_\tau \left| \sum_{i=1}^{3} v_i \nabla \phi_i \right|^p \tag{19}$$

$$= \frac{1}{p}\eta \, d\tau \left| \begin{bmatrix} \mathbf{D}_x \mathbf{v}_\tau \\ \mathbf{D}_y \mathbf{v}_\tau \end{bmatrix} \right|^p, \tag{20}$$

https://doi.org/10.5194/egusphere-2026-67
Preprint. Discussion started: 23 February 2026

with discretized gradient operators, $\mathbf{D}_x$ and $\mathbf{D}_y$, and strictly positive element area, $d\tau$. The discretized gradient operations are affine functions on element velocities, $\mathbf{v}_\tau$, which are convex. The norm operation is convex, followed by the power operation, which is convex for $p > 1$. Multiplication with strictly positive coefficients shows that $J_A(v_i)$ is convex.

Similarly, we decompose $J_B(v_i)$ on a single boundary edge, γ,

$$J_B(v_i) = \sum_{i=1}^{2} v_i \int_\gamma \tau_b(v)\phi_i \tag{21}$$

$$= \sum_{i=1}^{2} v_i \int_\gamma \tau_b(v_i) \tag{22}$$

$$= \sum_{i=1}^{2} v_i \, d\gamma \, \tau_b(v_i) \tag{23}$$

$$= d\gamma \boldsymbol{\tau}_b(\mathbf{v}_\gamma)^T \mathbf{v}_\gamma, \tag{24}$$

with nodal basal tractions, $\tau_b(v_i)$, and boundary edge length, $d\gamma$. Since $J_B(v_i)$ is convex on edge velocities, $\mathbf{v}_\gamma$, for basal tractions, $\tau_b(v) = |v|^m$ only when $m > 0$. This means that $J_B(v_i)$ remains convex only when the sliding law is perfectly-plastic, $m = 0$, or velocity-strengthening, $m > 0$, but not when we assume the unstable case of a velocity-weakening sliding law, $m < 0$.

Finally, $J_C(v_i)$ on a single element, τ, becomes

$$J_C(v_i) = -\rho g \sin\alpha \sum_{i=1}^{3} v_i \int_\tau \phi_i \tag{25}$$

$$= -f \, d\tau \, \mathbf{1}^T \mathbf{v}_\tau, \tag{26}$$

with driving stress, $f = \rho g \sin\alpha$. $J_C(v_i)$ is an affine function on element velocities, $\mathbf{v}_\tau$, and is therefore convex.

The summation of convex functions is convex, proving that the fully-discretized energy functional (i.e., the summation of each of these terms over all elements and boundary edges) is convex in v. Simplifying and vectorizing, the fully-discretized energy becomes

$$J(\mathbf{v}) = \frac{1}{p} \eta \, \mathbf{d}\boldsymbol{\tau}^T \, \|[\mathbf{D}_x\mathbf{v}, \mathbf{D}_y\mathbf{v}]\|^p + (\mathbf{d}\boldsymbol{\gamma} \circ \boldsymbol{\tau}_b)^T \mathbf{v}_b - (\mathbf{d}\boldsymbol{\tau} \circ \mathbf{f})^T \mathbf{v}, \tag{27}$$

with element-wise multiplication, $\circ$, boundary nodal values, $\cdot_b$, and second-dimension vector-wise norm, $\|\cdot\|$. Therefore, the fully-discretized energy functional is a convex function on the vectorized speed, $\mathbf{v}$.

The resulting vectorized, fully-discretized energy becomes,

$$J(\mathbf{u}) = \frac{1}{p} (\boldsymbol{\eta}(T) \circ \mathbf{d}\boldsymbol{\tau})^T \, \|[\mathbf{D}_x\mathbf{u}, \mathbf{D}_y\mathbf{u}]\|^p + (\mathbf{d}\boldsymbol{\gamma} \circ \boldsymbol{\tau}_b)^T \mathbf{u}_b - (\mathbf{d}\boldsymbol{\tau} \circ \mathbf{f})^T \mathbf{u}, \tag{28}$$

with discretized gradient operators, $\mathbf{D}_x$ and $\mathbf{D}_y$, element-wise multiplication, $\circ$, boundary nodal values, $\cdot_b$, and second-dimension vector-wise norm, $\|\cdot\|$. Therefore, the fully discretized energy functional is a convex function on the vectorized speed, $\mathbf{v}$.

https://doi.org/10.5194/egusphere-2026-67
Preprint. Discussion started: 23 February 2026

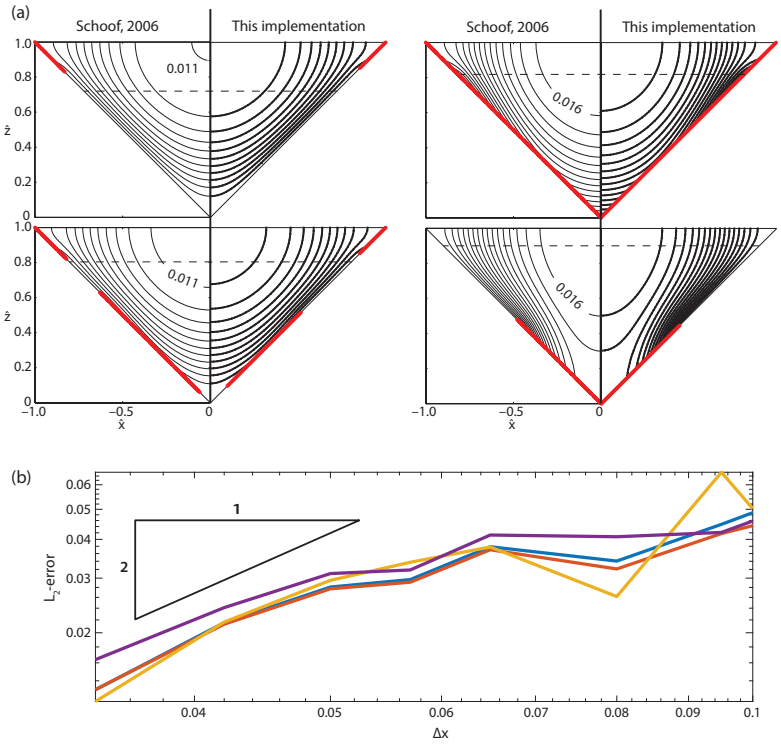

Figure 4. Verification of our numerical implementation of the mechanical model against Schoof (2006b). (a) Contours of flow speed for an idealized valley glacier as specified in Schoof (2006b). Mimicking Figure 5 in Schoof (2006b), the dashed line signifies the water table, with each flow regime chosen to exhibit markedly different regions of till failure (red lines). (b) Convergence plots of the normalized L_2-error on surface velocities, computed against the most refined solution with the four curves representing the four benchmark examples shown in (a) . We observe the expected second-order convergence of linear finite elements. Figure created by Cooper W. Elsworth.

A similar process applied to the thermal minimization problem in Eq. 14, results in a vectorized, fully-discretized energy,

$$L(\mathbf{T}) = \frac{1}{2}(\mathbf{k} \circ \mathbf{d}\boldsymbol{\tau})^T \left\| [\mathbf{D}_x\mathbf{T}, \mathbf{D}_y\mathbf{T}] \right\|^2 + G_{\text{geo}}\mathbf{d}\boldsymbol{\gamma}^T\mathbf{u}_b - (\mathbf{d}\boldsymbol{\tau} \circ \tau_E(\mathbf{T})\dot{\epsilon}_E(\mathbf{u}))^T\mathbf{T}. \tag{29}$$

We solve both minimization problems through the Disciplined Convex Programming software library, CVX (Grant and Boyd, 2014).

The governing equations are coupled through temperature-dependent ice viscosity, $\eta(T)$, and viscous shear heating, $2\tau_E(u)\dot{\epsilon}_E(u)$. We implement this coupling through an underrelaxed Newton-Raphson iteration between the thermal and mechanical models, as illustrated in Figure 3. At each iteration, we relax the thermal solution by a relaxation parameter, $\omega = [0, 1]$, and iterate until the residual falls below a threshold, ϵ. The result of this coupling is an antiplane speed u, and a temperature field T, which are fully consistent.

https://doi.org/10.5194/egusphere-2026-67
Preprint. Discussion started: 23 February 2026

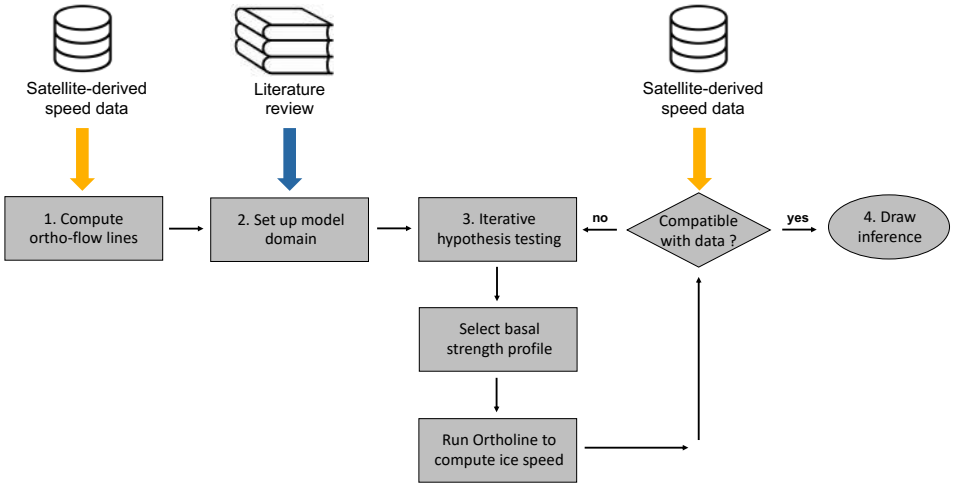

Figure 5. Flowchart for the application of Ortholine to a given field site. Each of the four main steps is discussed in detail in section 3. The only necessary data set for setting up the model is surface-speed data, typically derived from satellite-based measurements. Speed data is necessary for computing the direction of antiplane strain used to identify ortho-flow lines. Other data can be valuable to integrate (blue arrow), but only speed data is necessary (orange arrow).

2.3 Verification

To verify the accuracy of our implementation of the mechanical model, we benchmark against the analytical solution derived for an idealized valley glacier in Schoof (2006b). This test case consists of a simplified glacier valley geometry underlain by saturated sediments, with variable pore pressure resulting from a specified elevation of the water table. Different failure regions become apparent when the elevation of the water table and the driving stress are varied. Figure 4 a shows the model setup of a triangular computational domain, with the elevation of the water table denoted by a dashed line and the failure patches shown in red. In Figure 4a, we reproduce Figure 5 from Schoof (2006b) with the developed method by simulating the four distinct failure regimes. We demonstrate that our solver using a nominal grid spacing of Δx = 0.02 reproduces the velocity field and failure patches of Schoof (2006b). Small deviations between these two solutions likely result from differences in discretization parameters.

We perform a numerical convergence analysis of Ortholine for each of these benchmark solutions, shown in Figure 4b. The normalized L_2-error of the surface velocities, computed against the most refined simulation, exhibit second-order convergence with grid refinement. The linear finite elements lead to first-order accuracy, $p = 1$, with an expected $p + 1$, or second-order, numerical convergence rate (Brenner and Scott, 2007). The observed second-order numerical convergence makes us confident that our implementation of the numerical method is correct and consistent. We are not aware of a verification case of a thermomechanically coupled free-boundary problem that would allow us to perform a similar analysis for thermally variable ice.

https://doi.org/10.5194/egusphere-2026-67
Preprint. Discussion started: 23 February 2026

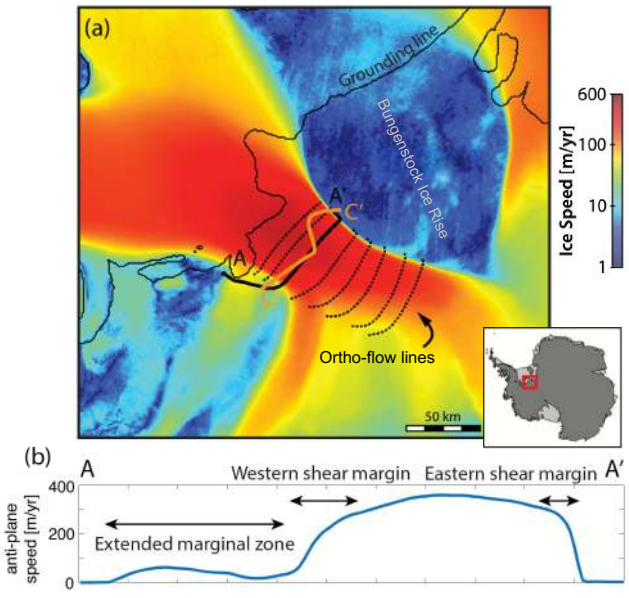

Figure 6. Identification of ortho-flow lines for Institute Ice Stream. (a) Map of ice speeds derived from satellite radar data (Rignot et al., 2011) and generated with the Antarctic Mapping Toolbox (Greene et al., 2017) with a set of numerically computed ortho-lines (dashed black lines) superimpsed. (b) We choose to focus on the ortho-flowline A-A' because of its proximity to the radar cross-section C-C' from Siegert et al. (2016). Figure created by Cooper W. Elsworth.

3 Application of Ortholine to a specific field site

Ortholine is intended as a general framework that can in principle be applied to any field site, where the properties of the shear margins are of specific interest. However, the model has more potential to lead to valuable scientific insights at field sites where the shear margin is only partially controlled by topography, where subglacial conditions are thought to vary, and where field observations are available to constrain bed conditions. Fig. 5 outlines the workflow for applying Ortholine to a given field site. We illustrate these steps below for the example of Institute Ice Stream located in the Ronne Ice Shelf region of West Antarctica.

3.1 Compute ortho-flow lines

The classical conceptualization of ice streams by Raymond (1996) posits a plug-like motion in the trunk of the ice stream bordered by two narrow shear margins on the sides, yielding a flow configuration that is symmetric around the center line of the stream. In that limit, a simple linear transect that is orthogonal to the main flow direction and cuts through both shear margins is in a state of anti-plane shear, as assumed in many idealized shear-margin models (Jacobson and Raymond, 1998; Suckale et al., 2014; Perol et al., 2015; Haseloff et al., 2015). Although there are examples of ice streams that fit this original conceptualization, such as Kamb Ice Stream (Elsworth and Suckale, 2016), the majority of field sites will not.

https://doi.org/10.5194/egusphere-2026-67
Preprint. Discussion started: 23 February 2026

To analyze shear-margin properties in the field, the first step is to compute the curves that represent the closest equivalent to the simple cross-sectional transect envisioned by Raymond (1996). We refer to this set of curves as ortho-flow lines to highlight that their orientation is orthogonal to the local direction of ice speed, implying that they correspond to isocontours of the velocity potential, $\phi(\nabla\phi = \mathbf{u}_d)$. We numerically generate ortho-flow lines from the velocity field derived from existing satellite data (Rignot et al., 2011). One challenge is noise in this velocity field, because it can lead to deviations from irrotational flow ($\nabla \times \mathbf{u}_d = 0$). If the flow is not irrotational, we cannot directly solve for the velocity potential. Instead, we compute ortho-flow lines through numerical integration starting from a seed point in the center of the ice stream, x_0. Velocity vectors are perpendicular to the ortho-flow line, which we generate from the stream center outward through Euler integration,

$$x_{i+1} = x_i + \Delta x \frac{\mathbf{u}_d^{\perp}(x_i)}{|\mathbf{u}_d^{\perp}(x_i)|} \tag{30}$$

with step size, Δx. The resolution of the computation is smaller than the resolution of the observed velocity field, $\mathbf{u}_d$. This procedure generates an ortho-flow line, $\mathbf{x}$, with a maximal anti-plane velocity component and a near-zero in-plane velocity component. When the downstream ice speed drops below 10 m/s, this approach becomes noisy and we extend the ortho-flow line linearly.

Figure 6a shows the set of computed ortho-flow lines cutting across the trunk of Institute Ice Stream as dashed black lines. They are approximately linear near the center line of the stream, highlighting that Institute partially abides by the original conceptualization of ice streams by Raymond (1996). However, as the ortho-flow line approaches the margins of the ice stream, they increasingly curve to partially align with the main flow direction, particularly near the western shear margin as highlighted by the ortho-flow line A-A' that we intentionally extend until ice speed drops below 10 m/s. The pronounced curvature of the ortho-flow lines in the western shear margin is the consequence of lateral influx of ice through several smaller tributaries visible in Fig. 6a. It highlights that the orto-flow line A-A' is dynamically coupled to stresses tens of kilometers further downstream through an extended marginal zone highlighted in Fig. 6b.

3.2 Set up the model domain

The Ortholine model domain represents one ortho-flow line. In principle, Ortholine could represent any ortho-flow line, but some ortho-flow lines might be more suitable than others. For example, it might not be ideal to select an ortho-flow line that crosses the grounding line, because grounding-line processes are not currently included in the model. Also, it can valuable to select an ortho-flow line where data from previous field campaigns can shed additional light on basal processes. While only surface-speed data set is strictly necessary for setting up Ortholine, other constraints could elevate the scientific contribution of the modeling. We illustrate this process through a short literature review for Institute Ice Stream.

At Institute, streaming ice is bounded to the east by Bungenstock Ice Rise, and fed from the west by tributaries from the Ellsworth Mountains (Ross et al., 2011, 2014). As evident from the ice-speed map in Figure 7a, the eastern shear margin near the Bungenstock Ice Rise is very sharp, but the western shear margin is much less localized (Scambos et al., 2004). This asymmetry on the surface is mirrored by different subglacial conditions at the base of the ice, with the eastern shear margin underlain by sediments and the western shear margin underlain by a hardrock bed, as inferred from the radar profile C-C'

https://doi.org/10.5194/egusphere-2026-67
Preprint. Discussion started: 23 February 2026

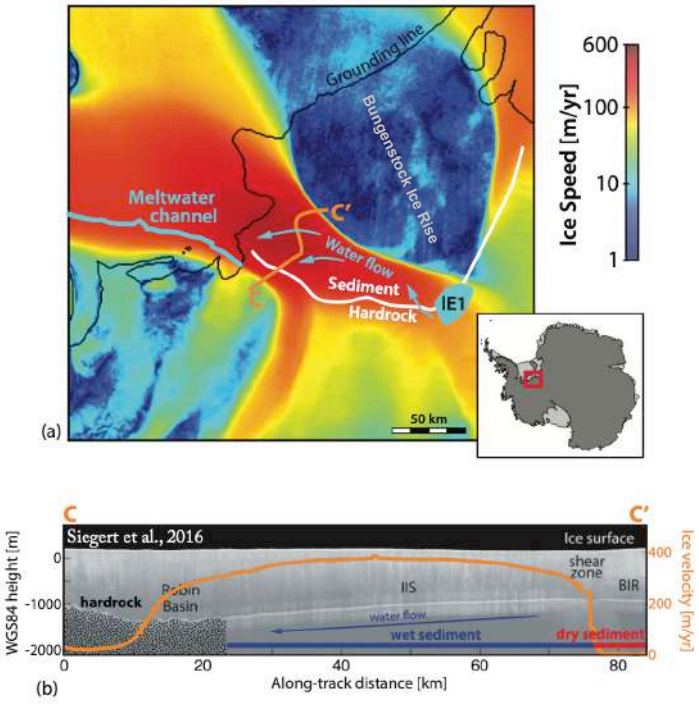

Figure 7. Observational constraints on subglacial conditions at Institute Ice Stream. (a) Map of the ice speed in the study area derived from satellite radar data (Rignot et al., 2011) and generated with the Antarctic Mapping Toolbox (Greene et al., 2017). The shear margins are the distinct lateral transitions from fast (red) to slow flow (blue). The inferred rock-sediment transition from Siegert et al. (2016) is indicated as a white line. We denote the main features of the subglacial hydrology in blue, including active subglacial lake (Smith et al., 2009), E1, hydropotential flow paths (Siegert et al., 2016), and a meltwater channel carved into the ice shelf (LeBrocq et al., 2013). (b) Radar cross-section along C-C' from Siegert et al. (2016), showing basal topography and inferred subglacial conditions. We superimpose the downstream ice speed as an orange line. Inferred hydropotential gradients (Siegert et al., 2016) suggest that water flow propagates from the shear margin on top of sediment to the shear margin on hardrock. Figure created by Cooper W. Elsworth.

shown in Figure 7b (Siegert et al., 2016). The basal topography across this profile is relatively subdued, making it unlikely that topographic control is the primary factor determining the shear margin position.

In the 2010-11 field season, the British Antarctic Survey completed extensive airborne geophysical surveys of the area, including radar sounding, gravity, magnetics, and LIDAR (Jordan et al., 2013). These geophysical data constrain the various factors that contribute to the dynamics of Institute Ice Stream, including topography, lithology, and hydrology. Siegert et al. (2016) highlight subglacial hydrology as an important factor that could induce rapid rearrangement in Institute's trunk. The trunk is downstream of an active subglacial lake, Institute E1 (Smith et al., 2009) highlighted in Figure 7a, and meltwater emanates from the western shear margin at the grounding line (LeBrocq et al., 2013; Alley et al., 2016) in the form of a channel. The hydraulic potential of Institute Ice Stream suggests that subglacial meltwater is routed from the eastern shear

https://doi.org/10.5194/egusphere-2026-67
Preprint. Discussion started: 23 February 2026

margin to the western shear margin (Siegert et al., 2016). The white line in Figure 7a represents a transition between subglacial sediments and hardrock, as inferred by Siegert et al. (2016) from seismic data.

For the remainder of this section, we choose to focus on ortho-flow line A-A', because of its proximity to the radar profile C-C' Siegert et al. (2016). At this location, the main ice stream trunk is approximately 60 kilometers wide and 1700 meters deep. We simplify the geometry of the actual bed profile by assuming a model domain with a flat surface and a bed that is piecewise-linear, neglecting roughness. The driving stress in the region is $f = \rho g H \sin\alpha = 27.5$ kPa, with ice density, $\rho = 917$ kg/m^3, acceleration due to gravity, $g = 9.8$ m/s^2, ice thickness, $H = 1275$ m, and surface slope, $\alpha = 0.0024$.

Based on the interpretation of radio-echo sounding data, Siegert et al. (2016) suggest that the lithology underneath Institute transitions from sediment to hardrock in the across-flow direction (see Fig. 7b). Both the bed roughness and the return power of the radio-echo sound provide evidence in favor of this interpretation (Siegert et al., 2016). We separate the bed into two boundary conditions specified by regions identified by Siegert et al. (2016) as hard rock and saturated sediments, respectively. Within the sediment-occupied zone, we impose a sharp increase in till strength outside of the eastern shear margin to represent a transition from temperate to frozen conditions, as inferred by Siegert et al. (2016).

The trunk of Institute Ice Stream (see Fig. 7) is underlain by a complex subglacial drainage system involving a lake upstream (Smith et al., 2009), lateral meltwater drainage in the main trunk, and a meltwater channel emanating from the grounding line in the vicinity of the western shear margin (LeBrocq et al., 2013). We assume that distributed drainage can be approximated as a thin film of meltwater and that efficient drainage occurs through a Röthlisberger channel (Röthlisberger, 1972) operating at low pore pressure (Hewitt, 2011; Perol et al., 2015; Elsworth and Suckale, 2016). The reduction in pore pressure in the vicinity of the channel depends on the channel discharge and the decay rate of the pressure perturbation scales with the film thickness of the distributed system, as derived in more detail in Perol et al. (2015).

We model the decline of bed strength away from a subglacial drainage located at Y as an exponential decline in the local pore pressure, p, with coefficient γ,

$$\tau_c(y) = f\left(\sigma_n - p\, e^{-|(y-Y)/\gamma|}\right) + c, \tag{31}$$

similar to a previous study of the effect of channelized drainage on shear margins (Elsworth and Suckale, 2016). Another factor modifying subglacial drainage in our domain is the variable overburden of the ice. The approximately linear basal topography across the trunk implies that ice thickness increases from approximately 1000 meters near the eastern to about 1700 meters near the western margin. We capture the effect of overburden pressure on the underlying hydrological system by assuming that the basal strength, τ_c, is a function of the pore pressure at the sliding interface, p:

$$\tau_c(y) = f(\rho g H(y) - p(y)) + c = C_f \rho g H(y)(1 - k_p) + c, \tag{32}$$

with friction parameter, $C_f \approx 0.5 - 0.6$ (Rathbun et al., 2008), sediment cohesion, $c \approx 1 - 2$ kPa (Kamb, 2001), and flotation fraction, k_p, which varies from 0 (no flotation) to 1 (full flotation).

https://doi.org/10.5194/egusphere-2026-67
Preprint. Discussion started: 23 February 2026

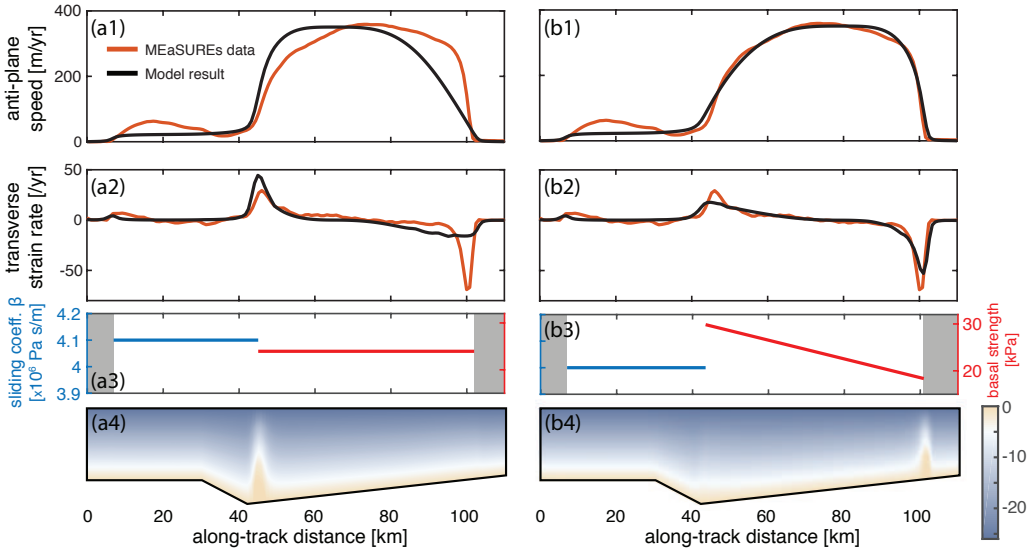

Figure 8. Numerical experiment investigating the relative importance of ice overburden. (a) Counterfactual simulation assuming uniform basal strength in the sediment indicative of ice overburden not being important. (b) Simulation assuming linearly increasing basal strength in the sediment as a function of overburden pressure. Rows illustrate: (1) Comparison of modeled velocities to observed MEaSUREs surface velocities across profile A-A'. (2) The modeled and observed strain rates across A-A'. (3) Tuned basal conditions, with locations specified from observations. Hardrock sliding parameter (blue), saturated sediment strength (red), and locked sediments (gray). (4) Temperature field in the ice column. Figure created by Cooper W. Elsworth.

3.3 Iterative hypothesis testing

The central idea of iterative hypothesis testing with Ortholine is that different basal processes generate distinct spatial profiles of basal strength, but only some of these profiles are consistent with observed surface velocities. For example, subglacial drainage can occur in multiple configurations (e.g., Flowers, 2015), each implying a different basal-strength profile. A channelized system would produce localized strengthening that decays away from the channel (Perol et al., 2015), whereas a distributed thin film would yield a more uniform bed strength. By testing which basal strength profiles reproduce measured surface speeds, Ortholine constrains which basal processes are plausible at a given field site.

In Figure 8, we illustrate how to test the hypothesis that basal strength underneath the fast-moving portion of Institute Ice Stream is dominated by ice overburden. We compare two simulations, one in which we assume that ice overburden does not affect the basal strength (panels a1-a4) and one in which ice overburden is the primary control (panels b1-b4). More specifically, we assume that the bed strength is constant for the simulation on the left, as would be the case if variable ice thickness did not matter. For the simulations on the right, we assume that pore pressure increases with ice overburden (see Eq. 32), leading

https://doi.org/10.5194/egusphere-2026-67
Preprint. Discussion started: 23 February 2026

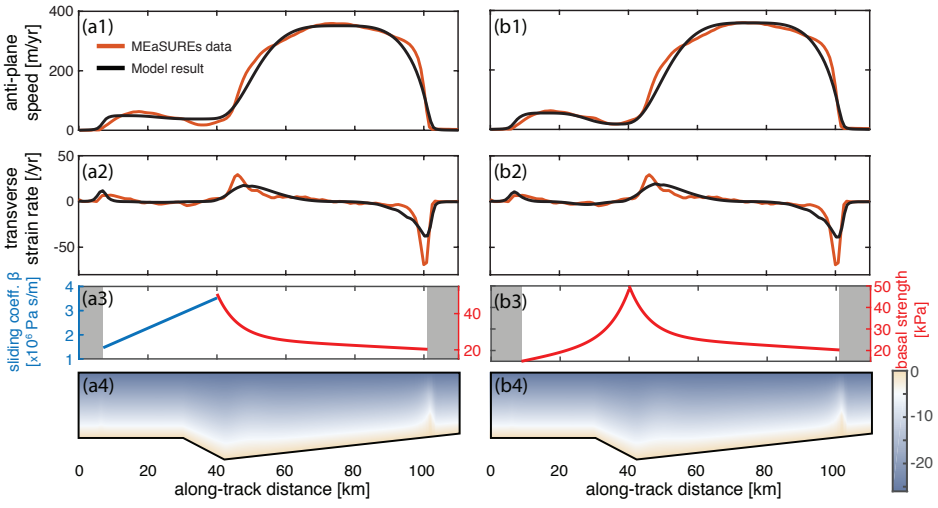

Figure 9. Numerical experiment to assess the relative importance of a channel located in the trough near the western shear margin. (a) Simulation assuming a hardrock ridge characterized by velocity-strengthening sliding over hard rock. (b) Counterfactual simulation assuming regularized Coulomb sliding in the extended marginal zone. Rows illustrate: (1) Comparison of modeled velocities to observed MEaSUREs surface velocities across profile A-A'. (2) The modeled and observed strain rates across A-A'. (3) Basal strength at the bed with hard rock sliding in blue and the basal strength of a plastic bed in red. (4) Temperature field in the ice column. Figure created by Cooper W. Elsworth.

to a linearly varying bed strength that is maximal at the topographic low. In both cases, we only show the simulation that best reproduces the observed surface speed.

For both simulations, the rows in Figure 8 show the calculated antiplane speed compared to the observed surface speed (panels a1 and b1), the calculated and observed transverse strain rates (panels a2 and b2), the sliding coefficient of the best fitting computation, β (panels a3 and b3) and the temperature distribution (panels a4 and b4). In both cases, we assume that the lithologic transition from rock (blue line in a3 and b3) to sediment (red line in a3 and b3) occurs in the vicinity of the western shear margin and that the ice trunk is bordered by areas of frozen basal conditions (shown in gray). In general, the computation based on the linear decrease in sediment strength from the western to the eastern shear margin fits observed surface speed much better (Figs. 8b1 vs a1). The best-fit strength profile varies linearly from 29.85 to 18.35 kPa across the ice stream trunk, mimicking the approximately linear basal topography across the trunk for an approximately constant average flotation factor of $k_p = 0.996$.

An interesting nuance of the analysis is that the ice overburden not only affects the basal strength, but also exhibits an indirect control on the englacial temperature, as evident in Figs. 8a4 and b4. The reason is that for the computation on the left (panels a1-a4), the sediment-portion of the bed is relatively weak and the hardrock-portion of the bed plays a more important role in the overall force balance. In comparison, sediment strength increases significantly from the eastern to the western shear margin for the computation on the right (panels b1-b4). The high basal strength in parts of the sediment portion means that the

https://doi.org/10.5194/egusphere-2026-67
Preprint. Discussion started: 23 February 2026

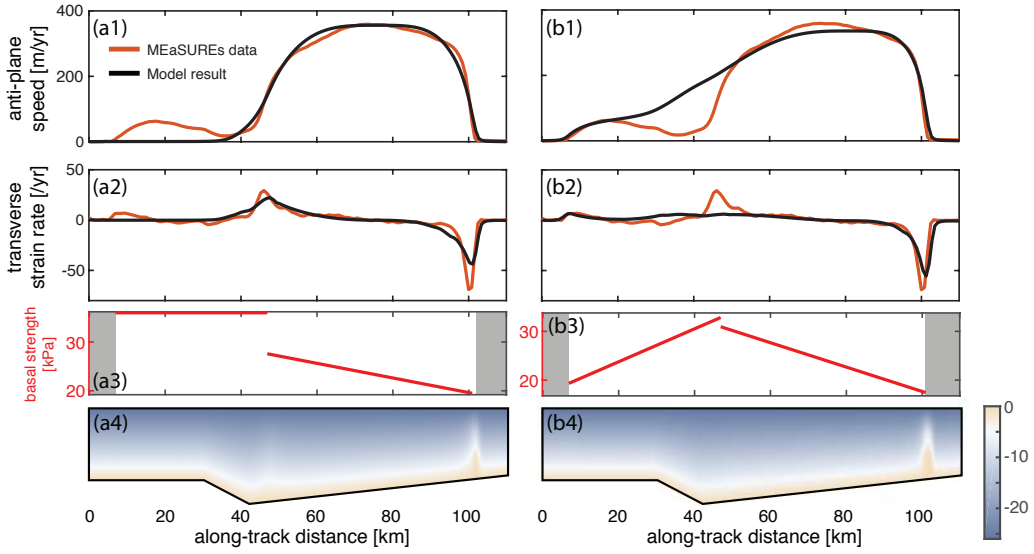

Figure 10. Counterfactual simulations assuming the absence of a meltwater channel near the western shear margin. (a) Simulation assuming that regularized Coulomb sliding over hardrock leads to approximately uniform basal strength. (b) Simulation assuming regularized Coulomb sliding with a linearly increasing basal strength in the extended marginal zone. Rows illustrate: (1) Comparison of modeled velocities to observed MEaSUREs surface velocities across profile A-A'. (2) The modeled and observed strain rates across A-A'. (3) Basal strength of the plasticly behaving bed. (4) Temperature field in the ice column. Figure created by Cooper W. Elsworth.

sliding coefficient of the rock portion of the bed is relatively lower, reducing shear heating near the western shear margin (see Fig. 8b4) compared to the case where the sliding coefficient is high in both segments (see Fig. 8a4).

Although Figure 8b1 fits the measured antiplane speed well for most of the ice-stream trunk, it reproduces the surface speed in the extended marginal zone less well. This disconnect suggests that a physical process other than ice overburden controls the basal strength distribution in the extended marginal zone. A likely candidate is subglacial hydrology, because the meltwater channel that emanates from below the western shear margin at the grounding line (see Fig. 7a) likely extends upstream into the trough near the western shear margin. The meltwater channel locally strengthens the bed (see Eq. 31), but little is known about how quickly the pressure perturbation induced by a meltwater channel decays spatially in the presence of both lithological and topographic variations. For a plastic bed, we assume a constant decay rate, γ, everywhere, implying that the channel alters the bed strength similarly irrespective of the lithology and local topography.

The existence of a meltwater channel near the western shear margin is well supported by observational data (e.g., see Fig. 7 and accompanying test). Less clear is how this meltwater channel affects basal strength. In Figure 9, we test the hypothesis that a channel leads to an exponential increase in basal strength near the western shear margin. We compare two simulations, our counterfactual represents classic, velocity-strengthening over hardrock (Figs. 9a1-a4) and the other assumes regularized Coulomb sliding (Figs. 9b1-b4). In the sediment-dominated portion of the domain, we superimpose the basal strengthening of

https://doi.org/10.5194/egusphere-2026-67
Preprint. Discussion started: 23 February 2026

the channel with a linear decrease in bed strength towards the eastern shear margin as a result of decreasing overburden (see Fig. 8). The agreement between the measured surface speed (Figs. 9 a1,b1) and the strain rate (Figs. 9 a2,b2) in the extended marginal zone improves significantly compared to Fig. 8. The quality of fit is comparable for both simulations, highlighting that both basal-strength distributions have comparable explanatory potential.

To create a counterfactual for Figure 9 that represents a scenario without a meltwater channel in the trough below the western shear margin, we assume that the presence of pervasive subglacial water leads to regularized Coulomb sliding in the hardrock portion of our model domain (Lliboutry, 1968; Iken, 1981; Fowler, 1986, 1987; Schoof, 2005; Gagliardini et al., 2007). In Figure 10, we test whether a plastic bed with variable strength improves the fit to observed surface speeds in the western shear margin and extended marginal zone. Similarly to Figure 8, we restrict our tests to constant and linearly varying basal strength profiles. To highlight that regularized Coulomb sliding is equivalent to plastic behavior of the bed, we plot both the hardrock and the sediment-dominated portion of the domain in red in Figure 10a3 and b3. Building on our analysis from Figure 8, we assume that the basal strength of the sediments decreases linearly from the western to the eastern shear margin.

The two best fitting simulations shown in Figure 10 demonstrate that switching the nature of sliding does not improve the fit to observed surface speed and strain rates. When assuming a constant basal strength, we are unable to reproduce the slow but finite sliding outside of the western shear margin (see Fig. 10a1). In comparison, velocity-strengthening sliding (see Fig. 8) is consistent with the observed slow slip. A linearly increasing basal strength profile provides a better fit in the extended marginal zone, but fails to capture the western shear margin (see Fig. 10b1 and b2). We emphasize that, contrary to Figure 8, it is also not clear why the basal strength in the extended marginal zone would increase linearly, because ice overburden does not vary much in the extended marginal zone.

3.4 Drawing inferences about the physical processes controlling shear-margin position and stability

Figure 8 suggests that the simplest hydrological system capable of reproducing the observed surface speed at Institute Ice Stream is a spatially well-connected drainage network near flotation. The simplest physical process that could explain the properties of this drainage network is variable ice overburden on a temperate bed with variable basal topography. Needless to say, there is almost certainly considerable small-scale variability not captured in Ortholine. However, this small-scale variability might not affect surface speed because ice acts as a low pass filter on basal topography and slipperiness, as analyzed in more detail in Gudmundsson (2003).

Transfer functions, pioneered by Gudmundsson (2003), are an approach to estimating the wavelength below which small-scale variability in basal topography or slipperiness is likely not relevant for surface velocities unless this small-scale variability is coupled with other basal processes. For example, a small topographic low with a meltwater channel within can still be dynamically relevant, not because of its own spatial scale but because of its large-scale effects on water routing. For example, the best fitting simulation shown in Figures 8b1-b4 entail a temperate zone in the eastern shear margin that could feed a meltwater channel causing local strengthening of the bed (Perol and Rice, 2015; Platt et al., 2016; Suckale et al., 2014; Elsworth and Suckale, 2016). Alternatively, the increase in bed strength could result from freezing (Schoof, 2004, 2012; Suckale et al., 2014; Perol et al., 2015; Haseloff et al., 2015). The latter explanation would require lateral advection of cold ice into the eastern

https://doi.org/10.5194/egusphere-2026-67
Preprint. Discussion started: 23 February 2026

shear margin to counteract the heating entailed in the measured strain rates (Figs. 8b2) and an additional englacial process like fabric to explain the narrow margin width.

Further evidence for the importance of small-scale variability in subglacial hydrology comes from Figure 9, which suggests that the basal strength distribution over the hardrock bed is dominated by the existence of a meltwater channel in or close to the western shear margin. However, Figure 8 demonstrates that the presence of this channel is not a necessary component to obtain a satisfactory fit to the surface speed and strain rates in most of the domain. This finding suggests that the channel is an important physical control for the western but not necessarily for the eastern shear margin. Given the pronounced lateral asymmetries in topography, lithology, and subglacial hydrology at Institute (see Sec. 3.2) it is maybe not surprising that the two shear margins could be controlled by different physical processes.

When drawing inferences about the physical processes controlling shear-margin properties through Ortholine, it is important to keep in mind that individual factors, such as topography, lithology, temperature, and subglacial hydrology, can be interconnected. This interconnectivity is the reason why it is challenging to derive insights into the physical processes controlling shear-margin properties from observational data alone, particularly for field sites like Institute where all of these factors vary simultaneously. Similarly, there may be large-scale variations that correlate with or follow a trend similar to overburden stress and are therefore difficult to differentiate from effects of ice thickness. We merely note here that it is not necessary to invoke this complexity in most of the domain for the model to be compatible with surface observables (Fig. 8b1).

To disentangle the various dependencies, Ortholine uses simple auxiliary assumptions (e.g., Eqs. 31 and 32) to link spatial variability in subglacial hydrology to specific physical processes such as ice overburden or the presence of a Röthlisberger channel. These auxiliary assumptions can be adjusted by the user. Generally, we recommend keeping the number of free parameters used in these auxiliary assumptions small to reduce the risk of overfitting. A similar strategy was recently used in Summers et al. (2023) to constrain the physical processes controlling shear-margin behavior at Thwaites, if in the context of a different model approach.

Ortholine is designed to evaluate the relative importance of different englacial and subglacial processes in controlling a specific shear-margin position. The main value of this insight for making inferences about future shear-margin stability lies in realizing that different physical processes evolve on different time scales. Topographically controlled shear margins are the most stable, the shear margin at Lambert Glacier being one example Sanderson et al. (2023). Thermal processes such as thawing of the subglacial bed can lead to shear-margin migration (Schoof, 2012) that is much faster than topographic change or erosion, but still comparatively slower than hydrological processes that can lead to sudden rearrangements of shear-margin position (Alley et al., 1994; Catania et al., 2006; Elsworth and Suckale, 2016).

4 Discussion

Different models have different strengths and weaknesses. Ice-sheet models such as the Ice Sheet System Model (Larour et al., 2012) or the Parallel Ice Sheet Model (Bueler and Brown, 2009) aim for realism by capturing the full two- or three-dimensional stress balance. They can represent lateral drag, tributary inflow, grounding line migration in complex geometries,

https://doi.org/10.5194/egusphere-2026-67
Preprint. Discussion started: 23 February 2026

but these advantages come at the cost of high computational demand and significant data requirements to constrain all model parameters (Kirchner et al., 2011). Flow-line models, by contrast, neglect lateral drag and assume simplified geometries, but are computationally efficient (Nye, 1952). They are tools for hypothesis testing by isolating a particular aspect of ice dynamics and focusing on analyzing its impact and have advanced our understanding of how longitudinal stress gradients change the transient responses of glaciers to external forcing (Pattyn, 2002) or how grounding-line stability varies with basal drag and rheology (Schoof, 2007).

Conceptually, Ortholine follows the modeling philosophy of flow-line models in which some aspects of ice dynamics are intentionally simplified or neglected to isolate the effect of others. It is also complementary to flow-line models. Instead of focusing on the longitudinal stress balance along a flow line while neglecting lateral effects, Ortholine focuses on lateral stresses while neglecting longitudinal effects. This model setup is useful for advancing our ability to identify how different physical processes affect shear-margin properties in the field.

Currently, evaluations of shear-margin stability are typically based on a qualitative comparison of whether the shear-margin coincides with distinctive topographic features or not (e.g., MacGregor et al., 2013; Sanderson et al., 2023). For example, MacGregor et al. (2013) argued that the eastern shear margin at Thwaites Glacier could be prone to migration because the topography below the eastern shear margin is flat (MacGregor et al., 2013). However, a more in-depth quantitative analysis of the shear margins at Thwaites (Summers et al., 2023) shows that this criterion alone is not sufficient to assess shear-margin stability. Many other processes affect shear-margin dynamics sensitively, from basal processes such as subglacial hydrology to regional-scale mass balance leading to rapid ice thinning at Thwaites (Smith et al., 2020).

Similarly, the presence of pronounced topography does not necessarily imply margin stability. For example, Summers et al. (2023) show that the western shear margin at Thwaites Glacier could also be prone to migration despite being located in an area of much more pronounced topography. Our simulations for Institute support this more nuanced view of shear-margin controls: Despite the fact that the western shear margin at Institute is approximately co-located with a topographic trough, our simulations suggest that the presence of a meltwater channel in this trough is important as evidenced by simulations with a meltwater channel (see Figs. 9a1 and b1) fitting observed surface speeds much better than simulations without a channel (see Figs. 10a1 and b1).

In addition to the inspiration we take from flow-line models, our model is motivated by the insights of previous anti-plane flow models of shear margins (Jacobson and Raymond, 1998; Schoof, 2004; Suckale et al., 2014; Perol and Rice, 2015; Haseloff et al., 2015; Elsworth and Suckale, 2016). At first, it might seem counterintuitive to adapt these highly idealized models to a particular field site, but this step is warranted by our advancing scientific understanding. We now have both observational (Harrison et al., 1998; Bindschadler and Vornberger, 1998; Echelmeyer and Harrison, 1999; Clarke et al., 2000; Catania et al., 2006) and theoretical evidence (Jacobson and Raymond, 1998; Schoof, 2004; Suckale et al., 2014; Perol and Rice, 2015; Haseloff et al., 2015; Elsworth and Suckale, 2016) that shear-margin migration is possible, in principle. The challenge now becomes to assess if and where shear-margin migration might occur not only in principle, but also in reality. This challenge is probably most acute for Thwaites Glacier MacGregor et al. (2013); Summers et al. (2023), but also relevant

https://doi.org/10.5194/egusphere-2026-67
Preprint. Discussion started: 23 February 2026

for other regions, such as Institute, where accelerated melting at the grounding line is expected later this century (Hellmer et al., 2012).

In addition to our growing scientific understanding, the design of field-site-specific shear-margin models through Ortholine is enabled by the substantial increase in the resolution of remotely detected data probing the ice sheets (Schroeder et al., 2014; Siegert et al., 2016; Muto et al., 2019; Koellner et al., 2019). Radio-echo sounding (Schroeder et al., 2014; Siegert et al., 2016) and seismic (Muto et al., 2019; Koellner et al., 2019) surveys have advanced our ability to map heterogeneities in subglacial conditions. These increasingly detailed observations highlight that heterogeneity in basal conditions is the norm rather than the exception. The observed diversity is not surprising in light of the numerous physical processes at play in a heterogeneous subglacial environment (Schroeder et al., 2014; Siegert et al., 2016; Muto et al., 2019; Koellner et al., 2019). Increasingly, these detailed observations provide an important opportunity for models to better constrain the relative importance of the various physical processes that contribute to the dynamics of ice streams and their shear margins.

5 Conclusions

In this paper, we develop Ortholine, a thermomechanical, antiplane strain model. Ortholine is designed to evaluate the relative importance of englacial and subglacial processes controlling shear-margin location. Building on the variational formulation by Schoof (2006a), we frame the problem in more flexible Disciplined Convex Programming (Grant et al., 2006)and implement a numerical solution using the software package CVX (Grant and Boyd, 2014). We verify our numerical implementation against the idealized mountain glacier case proposed by Schoof (2006b). We then illustrate the five key steps for applying the model to a given field site, using Institute Ice Stream as a proof-of-concept. Our simulations show that identifying the physical processes governing shear-margin stability through spatial association alone is not reliable. The presence of a topographic trough below a shear margin does not necessarily imply that the position of this shear margin is topographically controlled, as highlighted by the example of the western shear margin at Institute. Similarly, the presence of a gently sloping topography does not mean that topographic effects are irrelevant as demonstrated in Fig. 8. Ortholine provides a framework for evaluating the relative importance of different physical processes across an antiplane cross-section in a transparent, if simplified, way.

Code availability. Observational data including MEaSUREs surface velocity measurements and locations of subglacially sourced channels are publicly available through the National Snow & Ice Data Center (https://nsidc.org/data/). This code developed in this paper is open source for academic usage (https://github.com/coopere/InstituteIceStream2D) under the GNU General Public License, version 3. The specific version of the code (Elsworth and Shatty, 2025) used to create the results in this manuscript is archived at https://doi.org/10.5281/zenodo.18063098.

Author contributions. JS supervised the different stages of the study, participated in the conceptualization of the model, wrote the manuscript, and provided funding for all authors involved. CE led the early model and numerical method development stages, implemented the CVX-

https://doi.org/10.5194/egusphere-2026-67
Preprint. Discussion started: 23 February 2026

based version of the code, performed the verification analysis, and wrote the Methods section of the manuscript. All authors have reviewed and approved off the final version of the manuscript.

Competing interests. The authors declare that they have no conflicts of interest.

Acknowledgements. Ortholine was developed by Cooper W. Elsworth during his PhD at Stanford University. This research was supported by the National Science Foundation through the Office of Polar Programs awards PLR-1341499, PLR-1744758, and PLR-1739027. It benefited greatly from the input of Paul Summers, Neelanjan Akuli, Anuj Shetty, and Samantha Hordyk. The authors thank Dustin Schroeder, Neal Iverson, Lucas Zoet, Knut Christianson, and Mark Fahnestock for fruitful discussions.

https://doi.org/10.5194/egusphere-2026-67
Preprint. Discussion started: 23 February 2026

References

Alley, K. E., Scambos, T. A., Siegfried, M. R., and Fricker, H. A.: Impacts of warm water on Antarctic ice shelf stability through basal channel formation, Nature Geoscience, 9, https://doi.org/10.1038/ngeo2675, 2016.

Alley, K. E., Scambos, T. A., S., A. R., Rajaram, H., Pope, A., and Haran, T. M.: Continent-wide estimates of Antarctic strain rates from Landsat 8-derived velocity grids, Journal of Glaciology, pp. 1–12, https://doi.org/10.1017/jog.2018.23, 2018.

Alley, R. B., Anandakrishnan, S., Bentley, C. R., and Lord, N.: A water-piracy hypothesis for the stagnation of Ice Stream C, Antarctica, Annals of Glaciology, 20, 187–194, https://doi.org/10.3189/172756494794587032, 1994.

Bamber, J. L., Vaughan, D. G., and Joughin, I.: Widespread complex flow in the interior of the Antarctic ice sheet, Science, 287, 1248–1250, https://doi.org/10.1126/science.287.5456.1248, 2000.

Bindschadler, R. and Vornberger, P. L.: Changes in the West Antarctic Ice Sheet Since 1963 from Declassified Satellite Photography, Science, 279, 689–692, https://doi.org/10.1126/science.279.5351.689, 1998.

Bingham, R. G. and Siegert, M. J.: Radar-derived bed roughness characterization of Institute and Möller ice streams, West Antarctica, and comparison with Siple Coast ice streams, Geophysical Research Letters, 34, 1–5, https://doi.org/10.1029/2007GL031483, 2007.

Brenner, S. and Scott, R.: The mathematical theory of finite element methods, vol. 15, Springer Science & Business Media, 2007.

Bueler, E. and Brown, J.: Shallow shelf approximation as a "sliding law" in a thermomechanically coupled ice sheet model, Journal of Geophysical Research: Solid Earth, 114, 1–21, https://doi.org/10.1029/2008JF001179, 2009.

Catania, G. A., Scambos, T. A., Conway, H., and Raymond, C. F.: Sequential stagnation of Kamb Ice Stream, West Antarctica, Geophysical Research Letters, 33, 2–5, https://doi.org/10.1029/2006GL026430, 2006.

Clarke, T. S., Liu, C., Lord, N. E., and Bentley, C. R.: Evidence for a recently abandoned shear margin adjacent to ice stream B2, Antarctica, from ice-penetrating radar measurements, Journal of Geophysical Research: Solid Earth, 105, 13 409–13 422, https://doi.org/10.1029/2000JB900037, 2000.

Echelmeyer, K. and Harrison, W.: Ongoing margin migration of ice stream B, Antarctica, Journal of Glaciology, 45, 361–369, https://doi.org/10.3189/002214399793377059, 1999.

Elsworth, C. W. and Shatty, A.: Ortholine v1, https://doi.org/10.5281/zenodo.18063099, 2025.

Elsworth, C. W. and Suckale, J.: Rapid ice flow rearrangement induced by subglacial drainage in West Antarctica, Geophysical Research Letters, 43, https://doi.org/10.1002/2016GL070430, 2016.

Flowers, G. E.: Modelling water flow under glaciers and ice sheets, Proceedings of the Royal Society A: Mathematical, Physical and Engineering Sciences, 471, 20140 907, https://doi.org/10.1098/rspa.2014.0907, 2015.

Fowler, A.: A sliding law for glaciers of constant viscosity in the presence of subglacial cavitation, Proceedings of the Royal Society of London. A. Mathematical and Physical Sciences, 407, 147–170, https://doi.org/10.1098/rspa.1986.0090, 1986.

Fowler, A.: Sliding with cavity formation, Journal of Glaciology, 33, 255–267, https://doi.org/10.3189/S0022143000008820, 1987.

Friedman, A.: Variational principles and free-boundary problems, Courier Corporation, 2010.

Gagliardini, O., Cohen, D., Råback, P., and Zwinger, T.: Finite-element modeling of subglacial cavities and related friction law, Journal of Geophysical Research: Earth Surface, 112, https://doi.org/10.1029/2006JF000576, 2007.

Geuzaine, C. and Remacle, J.-F.: Gmsh: A three-dimensional finite element mesh generator with built-in pre- and post-processing facilities, International Journal for Numerical Methods in Engineering, 79, 1309–1331, https://doi.org/10.1002/nme.2579, 2009.

https://doi.org/10.5194/egusphere-2026-67
Preprint. Discussion started: 23 February 2026

Glen, J. W.: The creep of polycrystalline ice, Proceedings of the Royal Society of London. Series A. Mathematical and Physical Sciences, 228, 519–538, https://doi.org/10.1098/rspa.1955.0066, 1955.

Grant, M. and Boyd, S.: CVX: Matlab Software for Disciplined Convex Programming, version 2.1, https://cvxr.com/cvx/ [Last Accessed: 2026-01-05], 2014.

Grant, M., Boyd, S., and Ye, Y.: Disciplined Convex Programming, in: Global Optimization: From Theory to Implementation, edited by Liberti, L. and Maculan, N., pp. 155–210, Springer, Boston, MA, https://doi.org/10.1007/0-387-30065-1_7, 2006.

Greene, C. A., Gwyther, D. E., and Blankenship, D. D.: Antarctic Mapping Tools for MATLAB, Computers and Geosciences, 104, 151–157, https://doi.org/10.1016/j.cageo.2016.08.003, 2017.

Gudmundsson, G. H.: Transmission of basal variability to a glacier surface, Journal of Geophysical Research: Solid Earth, 108, https://doi.org/10.1029/2002JB002107, 2003.

Harrison, W., Echelmeyer, K., and Larsen, C.: Measurement of temperature in a margin of Ice Stream B, Antarctica: implications for margin migration and lateral drag, Journal of Glaciology, 44, 615–624, https://doi.org/10.3189/S0022143000002112, 1998.

Haseloff, M., Schoof, C., and Gagliardini, O.: A boundary layer model for ice stream margins, Journal of Fluid Mechanics, 781, 353–387, https://doi.org/10.1017/jfm.2015.503, 2015.

Haseloff, M., Hewitt, I., and Katz, R.: Englacial pore water localizes shear in temperate ice stream margins, Journal of Geophysical Research: Earth Surface, 124, 2521–2541, https://doi.org/10.1029/2019JF005399, 2019.

Hellmer, H. H., Kauker, F., Timmermann, R., Determann, J., and Rae, J.: Twenty-first-century warming of a large Antarctic ice-shelf cavity by a redirected coastal current, Nature, 485, 225–228, https://doi.org/10.1038/nature11064, 2012.

Hewitt, I. J.: Modelling distributed and channelized subglacial drainage: the spacing of channels, Journal of Glaciology, 57, 302–314, https://doi.org/10.3189/002214311796405951, 2011.

Holland, P. R., Bevan, S. L., and Luckman, A. J.: Strong ocean melting feedback during the recent retreat of Thwaites Glacier, Geophysical Research Letters, 50, https://doi.org/10.1029/2023GL103088, 2023.

Hooke, R. L., Raymond, C. F., Hotchkiss, R. L., and Gustafson, R. J.: Calculations of velocity and temperature in a polar glacier using the finite-element method, Journal of Glaciology, 24, 131–146, https://doi.org/10.3189/S0022143000014696, 1979.

Iken, A.: The effect of the subglacial water pressure on the sliding velocity of a glacier in an idealized numerical model, Journal of Glaciology, 27, 407–421, https://doi.org/10.3189/S0022143000011448, 1981.

Jacobson, H. and Raymond, C.: Thermal effects on the location of ice stream margins, Journal of Geophysical Research: Solid Earth, 103, 12 111–12 122, https://doi.org/10.1029/98JB00574, 1998.

Jamieson, S. S. R., Vieli, A., Livingstone, S. J., Cofaigh, C. Ó., Stokes, C., Hillenbrand, C.-D., and Dowdeswell, J. a.: Ice-stream stability on a reverse bed slope, Nature Geoscience, 5, 799–802, https://doi.org/10.1038/ngeo1600, 2012.

Jordan, T. A., Ferraccioli, F., Ross, N., Corr, H. F., Leat, P. T., Bingham, R. G., Rippin, D. M., le Brocq, A., and Siegert, M. J.: Inland extent of the Weddell Sea Rift imaged by new aerogeophysical data, Tectonophysics, 585, 137–160, https://doi.org/10.1016/j.tecto.2012.09.010, 2013.

Kamb, B.: Basal zone of the West Antarctic ice streams and its role in lubrication of their rapid motion, The West Antarctic ice sheet: behavior and environment, 77, 157–199, https://doi.org/10.1029/AR077p0157, 2001.

Kirchner, N., Hutter, K., Jakobsson, M., and Gyllencreutz, R.: Capabilities and limitations of numerical ice sheet models: A discussion for Earth-scientists and modelers, Quaternary Science Reviews, 30, 3691–3704, https://doi.org/10.1016/j.quascirev.2011.09.012, 2011.

https://doi.org/10.5194/egusphere-2026-67
Preprint. Discussion started: 23 February 2026

Koellner, S., Parizek, B., Alley, R., Muto, A., Holschuh, N., and Nowicki, S.: The impact of spatially-variable basal properties on outlet glacier flow, Earth and Planetary Science Letters, 515, 200–208, https://doi.org/10.1016/j.epsl.2019.03.026, 2019.

Larour, E., Seroussi, H., Morlighem, M., and Rignot, E.: Continental scale, high order, high spatial resolution, ice sheet modeling using the Ice Sheet System Model (ISSM), Journal of Geophysical Research: Earth Surface, 117, https://doi.org/10.1029/2011JF002140, 2012.

LeBrocq, A. M., Ross, N., Griggs, J. A., Bingham, R. G., Corr, H. F. J., Ferraccioli, F., Jenkins, A., Jordan, T. A., Payne, A. J., Rippin, D. M., and Siegert, M. J.: Evidence from ice shelves for channelized meltwater flow beneath the Antarctic Ice Sheet, Nature Geoscience, 6, 945–948, https://doi.org/10.1038/ngeo1977, 2013.

Lliboutry, L.: General theory of subglacial cavitation and sliding of temperate glaciers, Journal of Glaciology, 7, 21–58, https://doi.org/10.3189/S0022143000020396, 1968.

MacGregor, J. A., Catania, G. A., Conway, H., Schroeder, D. M., Joughin, I., Young, D. A., Kempf, S. D., and Blankenship, D. D.: Weak bed control of the eastern shear margin of Thwaites Glacier, West Antarctica, Journal of Glaciology, 59, 900–912, https://doi.org/10.3189/2013JoG13J050, 2013.

Meyer, C. R. and Minchew, B. M.: Temperate ice in the shear margins of the Antarctic Ice Sheet: Controlling processes and preliminary locations, Earth and Planetary Science Letters, 498, 17–26, https://doi.org/10.1016/j.epsl.2018.06.028, 2018.

Morland, L. and Johnson, I.: Steady motion of ice sheets, Journal of Glaciology, 25, 229–246, https://doi.org/10.3189/S0022143000010467, 1980.

Muto, A., Anandakrishnan, S., Alley, R. B., Horgan, H. J., Parizek, B. R., Koellner, S., Christianson, K., and Holschuh, N.: Relating bed character and subglacial morphology using seismic data from Thwaites Glacier, West Antarctica, Earth and Planetary Science Letters, 507, 199–206, https://doi.org/10.1016/j.epsl.2018.12.008, 2019.

Nye, J. F.: The mechanics of glacier flow, Journal of Glaciology, 2, 82–93, https://doi.org/10.3189/S0022143000033967, 1952.

Nye, J. F.: The distribution of stress and velocity in glaciers and ice-sheets, Proceedings of the Royal Society of London. Series A. Mathematical and Physical Sciences, 239, 113–133, https://doi.org/10.1098/rspa.1957.0026, 1957.

Pattyn, F.: Transient glacier response with a higher-order numerical ice-flow model, Journal of Glaciology, 48, 467–477, https://doi.org/10.3189/172756502781831278, 2002.

Perol, T. and Rice, J. R.: Shear heating and weakening of the margins of West Antarctic ice streams, Geophysical Research Letters, 42, 3406–3413, https://doi.org/10.1002/2015GL063638, 2015.

Perol, T., Rice, J. R., Platt, J. D., and Suckale, J.: Subglacial hydrology and ice stream margin locations, Journal of Geophysical Research, 120, 1–17, https://doi.org/10.1002/2015JF003542, 2015.

Platt, J. D., Perol, T., Suckale, J., and Rice, J. R.: Determining conditions that allow a shear margin to coincide with a Röthlisberger channel, Journal of Geophysical Research: Earth Surface, 121, 1273–1294, https://doi.org/10.1002/2015JF003707, 2016.

Rathbun, A. P., Marone, C., Alley, R. B., and Anandakrishnan, S.: Laboratory study of the frictional rheology of sheared till, Journal of Geophysical Research: Earth Surface, 113, https://doi.org/10.1029/2007JF000815, 2008.

Raymond, C.: Shear margins in glaciers and ice sheets, Journal of Glaciology, 42, 90–102, https://doi.org/10.3198/1996JoG42-140-90-102, 1996.

Reeh, N. and Paterson, W.: Application of a flow model to the ice-divide region of Devon Island ice cap, Canada, Journal of Glaciology, 34, 55–63, https://doi.org/10.3189/S0022143000009060, 1988.

Rignot, E., Mouginot, J., and Scheuchl, B.: Ice flow of the Antarctic ice sheet, Science, 333, 1427–1430, https://doi.org/10.1126/science.1208336, 2011.

https://doi.org/10.5194/egusphere-2026-67
Preprint. Discussion started: 23 February 2026

Ross, N., Siegert, M. J., Woodward, J., Smith, A. M., Corr, H. F., Bentley, M. J., Hindmarsh, R. C., King, E. C., and Rivera, A.: Holocene stability of the Amundsen-Weddell ice divide, West Antarctica, Geology, 39, 935–938, https://doi.org/10.1130/G31920.1, 2011.

Ross, N., Bingham, R., Corr, H. F. J., Ferraccioli, F., Jordan, T., Le Brocq, A., Rippin, D., Young, D., Blankenship, D., and Siegert, M. J.: Steep reverse bed slope at the grounding line of the Weddell Sea sector in West Antarctica, Nature Geoscience, 5, 393–396, https://doi.org/10.1038/ngeo1468, 2012.

Ross, N., Jordan, T. A., Bingham, R. G., Corr, H. F. J., Ferraccioli, F., Brocq, A. L., Rippin, D. M., Wright, A. P., and Siegert, M. J.: The ellsworth subglacial highlands: Inception and retreat of the west Antarctic ice sheet, Bulletin of the Geological Society of America, 126, 3–15, https://doi.org/10.1130/B30794.1, 2014.

Röthlisberger, H.: Water pressure in intra-and subglacial channels, Journal of Glaciology, 11, 177–203, https://doi.org/10.3189/S0022143000022188, 1972.

Sanderson, R. J., Winter, K., Callard, S. L., Napoleoni, F., Ross, N., Jordan, T. A., and Bingham, R. G.: Englacial architecture of Lambert Glacier, East Antarctica, The Cryosphere Discussions, 2023, 1–28, https://doi.org/10.5194/tc-17-4853-2023, 2023.

Scambos, T., Bohlander, J., Raup, B., and Haran, T.: Glaciological characteristics of Institute Ice Stream using remote sensing, Antarctic Science, 16, 205–213, https://doi.org/10.1017/S0954102004001919, 2004.

Schoof, C.: On the mechanics of ice-stream shear margins, Journal of Glaciology, 50, 208–218, https://doi.org/10.3189/172756504781830024, 2004.

Schoof, C.: The effect of cavitation on glacier sliding, Proceedings of the Royal Society A: Mathematical, Physical and Engineering Sciences, 461, 609–627, 2005.

Schoof, C.: A variational approach to ice stream flow, Journal of Fluid Mechanics, 556, 227, https://doi.org/10.1017/S0022112006009591, 2006a.

Schoof, C.: Variational methods for glacier flow over plastic till, Journal of Fluid Mechanics, 555, 299, https://doi.org/10.1017/S0022112006009104, 2006b.

Schoof, C.: Ice sheet grounding line dynamics: Steady states, stability, and hysteresis, Journal of Geophysical Research, 112, F03S28, https://doi.org/10.1029/2006JF000664, 2007.

Schoof, C.: Thermally driven migration of ice-stream shear margins, Journal of Fluid Mechanics, 712, 552–578, https://doi.org/10.1017/jfm.2012.438, 2012.

Schroeder, D. M., Blankenship, D. D., Young, D. a., and Quartini, E.: Evidence for elevated and spatially variable geothermal flux beneath the West Antarctic Ice Sheet, Proceedings of the National Academy of Sciences, 2014, 3–5, https://doi.org/10.1073/pnas.1405184111, 2014.

Siegert, M. J., Ross, N., Li, J., Schroeder, D. M., Rippin, D., Ashmore, D., Bingham, R., and Gogineni, P.: Subglacial controls on the flow of Institute Ice Stream, West Antarctica, Annals of Glaciology, 57, 19–24, https://doi.org/10.1017/aog.2016.17, 2016.

Smith, B., Fricker, H. A., Gardner, A. S., Medley, B., Nilsson, J., Paolo, F. S., Holschuh, N., Adusumilli, S., Brunt, K., Csatho, B., et al.: Pervasive ice sheet mass loss reflects competing ocean and atmosphere processes, Science, 368, 1239–1242, https://doi.org/10.1126/science.aaz5845, 2020.

Smith, B. E., A. Fricker, H., Joughin, I. R., and Slawek, T.: An inventory of active subglacial lakes in Antarctica detected by ICESat (2003-2008, Journal of Glaciology, 55, 573–595, https://doi.org/10.3189/002214309789470879, 2009.

Suckale, J., Platt, J. D., Perol, T., and Rice, J. R.: Deformation-induced melting in the margins of the West Antarctic ice streams, Journal of Geophysical Research, 119, 1004–1025, https://doi.org/10.1002/2013JF003008, 2014.

https://doi.org/10.5194/egusphere-2026-67
Preprint. Discussion started: 23 February 2026

Summers, P. T., Elsworth, C. W., Dow, C. F., and Suckale, J.: Migration of the shear margins at Thwaites Glacier: Dependence on basal conditions and testability against field data, Journal of Geophysical Research: Earth Surface, 128, https://doi.org/10.1029/2022JF006958, 2023.

Thomas, R. H.: The dynamics of marine ice sheets, Journal of Glaciology, 24, 167–177, https://doi.org/10.3189/S0022143000014726, 1979.

Tulaczyk, S., Kamb, W. B., and Engelhardt, H. F.: Basal mechanics of Ice Stream B, west Antarctica: 2. Undrained plastic bed model, Journal of Geophysical Research, 105, 483, https://doi.org/10.1029/1999JB900328, 2000a.

Tulaczyk, S., Kamb, W. B., and Engelhardt, H. F.: Basal mechanics of Ice Stream B, west Antarctica: 1. Till mechanics, Journal of Geophysical Research, 105, 463, https://doi.org/10.1029/1999JB900329, 2000b.

Weertman, J.: On the sliding of glaciers, Journal of Glaciology, https://doi.org/10.1007/978-94-015-8705-119, 1957.

Weertman, J.: Stability of the junction of an ice sheet and an ice shelf, Journal of Glaciology, 13, 3–11, https://doi.org/10.3189/S0022143000023327, 1974.

Zoet, L. K. and Iverson, N. R.: Rate-weakening drag during glacier sliding, Journal of Geophysical Research: Earth Surface, 121, 1206–1217, https://doi.org/10.1002/2016JF003909, 2016.